Conference on Modelling Fluid Flow (CMFF'25)
The 19th International Conference on Fluid Flow Technologies
Budapest, Hungary, August 26 - August 29, 2025

APPLICATION RANGES OF THE HAGEN-POISEUILLE LAW TO MODEL NON-NEWTONIAN FLUID-FILLED DAMPERS

Boglárka BALOG[1], Péter NAGY-GYÖRGY[2]

[1] Corresponding Author. Department of Hydrodynamic Systems, Faculty of Mechanical Engineering, Budapest University of Technology and Economics. Bertalan Lajos u. 4 – 6, H-1111 Budapest, Hungary. E-mail: bbalog@hds.bme.hu
[2] Department of Hydrodynamic Systems, Faculty of Mechanical Engineering, Budapest University of Technology and Economics. E-mail: nagy-gyorgy.peter@gpk.bme.hu

ABSTRACT

Non-Newtonian liquids, such as magnetorheological and shear thickening fluids, are increasingly utilized in hydraulic dampers due to better controllability and energy absorption capabilities. Despite these advantages, the design of such dampers remains heavily reliant on empirical experiments, and accurately modelling their damping characteristics presents a persistent challenge. The most common method involves applying the Hagen-Poiseuille law to describe the flow inside the damping channel, and the damping force is calculated from the pressure drop. However, in several practical scenarios, this approach may lead to significant inaccuracies due to the simplifications. We aim to describe the application range, where the law can predict the damping characteristic with reasonable accuracy. We performed steady state CFD simulations with different dimensions and frequencies for Newtonian, and shear thickening fluids. The results were compared to the analytical values, and the relative error was plotted using the function of dimensionless length/diameter ratio. Based on the contour plots, the industry can identify the ranges where the approximations are applicable.

Keywords: CFD, damper modelling, Hagen-Poiseuille law, non-Newtonian fluid, shear thickening fluid

NOMENCLATURE

A	$[m^2]$	piston surface
d	$[m]$	piston diameter
D	$[m]$	outer cylinder diameter
f	[-]	function
F	$[N]$	load
L	$[m]$	channel length
p	$[Pa]$	pressure
Q	$[m^3/s]$	volume flow rate
R	$[m]$	radius
t	$[s]$	time
u	$[m/s]$	velocity component in x direction
v	$[m/s]$	velocity component in y direction
w	$[m/s]$	velocity component in z direction
$\dot{\gamma}$	[1/s]	shear rate
η	$[Pa{\cdot}s]$	dynamic viscosity
τ	$[Pa]$	shear stress

Subscripts and Superscripts

c	critical
max	maximum
w	wall

Abbreviation

STF	shear thickening fluid
CFD	computational fluid dynamics
PL	power-law
PEG	polyethylene glycol

1. INTRODUCTION

Shear thickening fluids (STFs) are increasingly used in hydraulic dampers due to their self-adaptive characteristics and enhanced energy absorption capabilities. However, the accurate prediction of damping characteristics, $F(v)$, remains a significant challenge. In engineering practice, the damping force is commonly estimated using analytical models based on the Hagen-Poiseuille law, which assumes laminar, Newtonian flow through the orifices. While this approach provides a convenient first approximation, its validity for STF-based dampers has not been systematically established, raising concerns about its accuracy in practical applications.

Existing methods for determining damping characteristics rely heavily on experiments [1–6], but the measured data could be compared only to analytical solutions derived from Newtonian [2] or traditional non-Newtonian rheological models such as power law [7] or Herschel-Bulkley [8]. However, these models frequently fail to account for the

distinctive three region viscosity curve of STFs, leading to inaccuracies in predicted damping forces. Furthermore, numerical simulations such as computational fluid dynamics (CFD) provide precise solutions but are computationally expensive and constrained by predefined rheological models (e.g., Newtonian, Bingham, power-law, Herschel-Bulkley, Carreau-Yasuda models) [9].

To address these limitations, our previous study [10] introduced an analytical method for estimating damping characteristics without relying on rheological model fitting. Instead, we directly incorporated measured rheological data, enabling an inverse approach to identify appropriate fluid properties for a given damping requirement. The derivation based on the Hagen-Poiseuille law for pipe flow applying assumption that the entrance and exit losses are negligible compared to the viscous flow losses, so the pipes are sufficiently long to have a fully developed flow. The CFD results prove the accuracy of the novel analytical model when the assumptions are fulfilled.

Our initial validation of these assumptions was performed for power-law (PL) and STF rheologies [10], where parameter sweeps were conducted for cylindrical orifice geometries. Although 3D simulations with multiple orifices provided accurate results [11], they were computationally demanding, leading us to adopt a 2D simplification for broader parameter exploration.

Building on these prior investigations, the present study systematically assesses the validity of the Hagen-Poiseuille law in predicting STF damping characteristics by comparing the CFD and analytical results. The primary objective is to identify the applicability range of this law and quantify deviations beyond its valid range. To achieve this, we map the relative error as a function of the dimensionless length-to-diameter ratio and relative volume flow rate. While previous research has examined the effects of various rheological models, the specific transition boundaries where Hagen-Poiseuille-based predictions break down remain poorly defined. By providing a detailed error analysis and visualization, this study establishes an industry-relevant framework for determining when these simplifications hold, thus guiding the design of STF-based dampers with greater accuracy.

A critical aspect of ensuring the accuracy of these investigations is the reliability of the rheological data used as input for both analytical and numerical models. However, existing studies report significantly different rheological properties for STFs with identical compositions, suggesting inconsistencies in measurement techniques or variations in experimental conditions [12,13]. Under controlled conditions, we synthesized STF samples to ensure consistency in rheological measurements, providing reliable input data for both analytical and numerical models. Building on this foundation, this study systematically evaluates the applicability of the Hagen-Poiseuille law in predicting STF-based damper behaviour by comparing analytical predictions with CFD simulations. We examine a range of flow conditions and geometries to identify the accuracy limits of the analytical approach and quantify deviations beyond its valid range. By analysing the relationship between relative error, dimensionless parameters, and flow characteristics, we establish guidelines for when the Hagen-Poiseuille approximation remains valid. The findings offer practical insights for damper design, highlighting the importance of precise rheological characterization and the conditions under which simplified models can be confidently applied.

2. MATERIALS AND METHODS

2.1. Materials and Experimental Procedures

2.1.1. Materials

The STF is composed of nanoscale silica particles suspended in a carrier liquid. The fumed silica (Aerosil® R816, provided by Evonik) has a primary particle size of 12 nm and a specific surface area of approximately 190 ± 20 m^2/g [14]. The silica is post-treated with hexadecylsilane, consisting of slightly hydrophobic, spherical particles. Due to its large surface area and porous structure, R816 silica effectively adsorbs gases, liquids, and other substances. This type of silica is characterized by an extremely fine powder form. Its key advantages include excellent dispersibility, enabling homogeneous distribution in various media and enhancing product performance. Furthermore, it offers high thermal stability and chemical resistance, making it suitable for applications across a wide temperature range and in oxidative or corrosive environments. The carrier liquid used in the formulation was polyethylene glycol with a molecular weight of 200 g/mol (PEG 200, product code P0840, supplied by TCI Chemicals). It is a colourless, clear liquid but has lower viscosity and is miscible with water. Due to its low viscosity and miscibility, it is advantageous in applications where easy blending or compatibility with other substances is essential.

2.1.2. Sample preparation

During the preparation process, the liquid medium and silica were introduced in alternating increments, each constituting one-third of the total required volume. Following each addition, the sealed bottles were subjected to ultrasonication for 30 minutes to promote dispersion. This process was repeated twice to ensure uniform distribution of the silica within the medium. Subsequently, the sealed bottles were placed in a water bath and gradually heated to 80 °C. Upon reaching the target

temperature, the bottle caps were removed, and the samples were subjected to continuous stirring for 2 hours using an overhead stirrer to achieve thorough homogenization. As a result, a transparent and homogeneous fluid was obtained. For each STF, specific quantities of fumed silica were incorporated into the carrier fluid at a defined weight fraction (12 and 15 wt.%).

2.1.3. Rheological measurements

An Anton Paar MCR 301 rotational rheometer equipped with a cone-plate measuring system was used to determine the rheological properties of the STF samples. The measuring system featured a cone with a diameter of 25 mm and a fixed gap of 0.054 mm, ensuring precise control of the measurement parameters. Based on the defined gap distance, the applied force, and the rotational speed, the instrument recorded and plotted shear rate versus viscosity data. The suspensions were analysed within a shear rate range of 0.1 to 10,000 s^{-1}. All measurements were carried out at a constant temperature of 25°C to ensure accuracy and reproducibility.

2.2. Analytical approach

Rheological measurements provided shear rate and shear stress data, which can be used to estimate the expected velocity-pressure drop function for a given system. The analytical approach presented in this section is based on the methodology detailed in [10], where a comprehensive derivation and validation using CFD simulations can be found. By utilizing these relationships, a predictive framework is established for describing the flow behaviour of the dilatant fluid under given operating conditions.

The hydraulic dampers usually characterised by the *F(v)* force(velocity) characteristic. When the piston with surface A_{piston} moves with a v_{piston} velocity, the liquid flows through the gap with the

$$Q = v_{piston}\, A_{piston} \tag{1}$$

volume flow rate. The Δp pressure difference between the chambers drives the flow, which is proportional to the compressing force, since

$$F = \Delta p\, A_{piston} \tag{2}$$

As a result, we can see that the *Q*-Δp relationship is essential to predict the *F(v)* damping characteristic.

To develop the analytical model, laminar flow was assumed as in the similar research studies such as [15,16]. The governing equations are the momentum and the continuity equation in a cylindrical coordinate system (x, r, θ) applying the assumptions:

1. The fluid is incompressible.
2. The solution corresponds to a steady-state condition with no time dependence.
3. The flow is two-dimensional, meaning all quantities are constant in the θ direction.
4. The axial velocity component u depends only on the radial coordinate ($u = u(r)$), while the other velocity components are zero ($v = w = 0$).
5. The pressure gradient is constant.

With these assumptions, the continuity equation and the momentum equation in the θ tangential and in x longitudinal directions are automatically satisfied. The remaining simplified equation is the

$$0 = -\frac{dp}{dx} + \frac{1}{r}\frac{d}{dr}(r\tau) \tag{3}$$

with the

$$u(r = R) = 0 \tag{4}$$

boundary condition, where $\tau(r)$ represents the local shear stress in the function of the radial coordinate. This equation is valid for any shear rate–shear stress rheology $\tau = g(\dot{\gamma})$. After integrating with respect to r, the local shear stress is

$$\tau = \frac{dp}{dx}\frac{r}{2} + \tau_0, \tag{5}$$

For arbitrary non-Newtonian rheology, where τ_0 is the local shear stress at the centreline of the pipe. Since the bore and, consequently, the flow is axisymmetric, it follows that $\tau_0 = 0$.

Based on these considerations, the volumetric flow rate can be determined using the following equation:

$$Q = \frac{2\pi R^3}{{\tau_w}^3}\left[\frac{{\tau_w}^2}{2}F(\tau_w) - S(\tau_w)\right], \tag{6}$$

where R is the radius, L is the channel length, $\tau_w = \frac{dp}{dx}\frac{R}{2} = \frac{\Delta p R}{2L}$ is the wall shear stress, and

$$F(\tau) = \int_0^{\tau} f(\tilde{\tau})\, d\tilde{\tau} \tag{7}$$

$$S(\tau) = \int_0^{\tau} \tilde{\tau} F(\tilde{\tau})\, d\tilde{\tau} \tag{8}$$

are integral functions where $f(\tau) = g^{-1}(\tau)$ represents the inverse function of the traditional shear stress-shear rate rheological curve.

The authors would emphasize that this method does not require any model fittings, since the integrations in Eq. (7) and (8) can be performed numerically (e.g. with trapezoidal method) using the measurement data directly. Rearranging eq. (6) gives the

$$\tilde{Q} := \frac{Q}{2\pi R^3} = \frac{1}{{\tau_w}^3}\left[\frac{{\tau_w}^2}{2}F(\tau_w) - S(\tau_w)\right], \tag{9}$$

relative flow rate, which depends only on the τ_w wall shear stress. It practically means that the $\tilde{Q}$ - τ_w curve depends only on $f(\tau)$ inverse rheological curve. Since this curve does not depend on the geometric dimensions, we will define the volume flow rate to have uniformly distributed $\tilde{Q}$ values in the range of 10-10000 1/s.

The Eq. (9) has a simpler form for Newtonian case,

$$\tilde{Q} := \frac{\tau_w}{8\eta} \tag{10}$$

when the inverse rheological and the integral functions are

$$f(\tau) = \frac{\tau}{\eta}, \qquad F(\tau) = \frac{\tau^2}{2\eta}, \qquad S(\tau) = \frac{\tau^4}{8\eta} \quad (11)$$

and η is the Newtonian dynamic viscosity.

2.3. CFD setup

To evaluate the accuracy of the Hagen-Poiseuille law in predicting the damping characteristics of non-Newtonian fluids in hydraulic dampers, CFD simulations were performed using OpenFOAM (Version 2112, [17]). The study focused on a single damping channel geometry for various length and diameter configurations. Consistent material properties, boundary conditions, and numerical settings were applied across all cases. The objective was to determine the range of validity for the analytical approach by comparing the CFD results to theoretical predictions.

2.3.1. Geometry and meshing

Fig. 1 show the computational domain. To reduce computational cost while maintaining accuracy, a two-dimensional axisymmetric approach was employed, where only a 5° wedge of the circular domain was modelled. The mesh was generated using the built-in *blockMesh* utility, which decomposes the domain into structured hexahedral elements. Mesh parameters, including nodal coordinates, division counts, and expansion ratios, were computed using a custom MATLAB script to ensure a high-quality structured mesh with minimal distortion. The resulting mesh was composed entirely of hexahedral elements, exhibiting zero non-orthogonality and a maximum skewness of 0.320537.

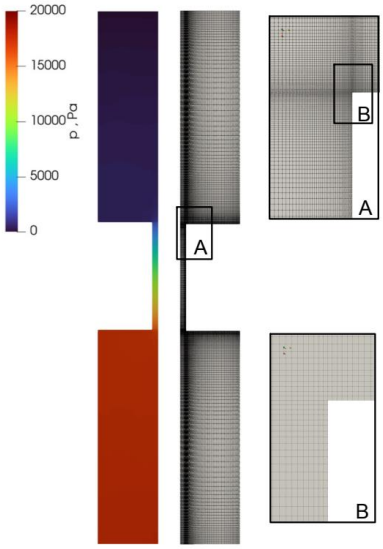

Figure 1. The mesh of the investigated damper and the corresponding pressure distribution

To assess the influence of discretization errors, a mesh independence study was performed by evaluating four different mesh densities: 21.2k, 51.2, 132.6k, and 341.4k elements. The study considered the effects of gap size variations and the shear-thickening rheology by analysing two different diameters, 11 different lengths, 15 different velocities and three rheological models in all combinations. As a result, 2x11x15x3 = 1320 steady state simulations were performed. Mesh independence analysis was performed based on the maximum volume flow rate, and the relative difference in the computed force values was found to be less than 1% between the three finest meshes. Consequently, the mesh with 133.4k cells was selected for all subsequent simulations (see Fig. 1).

2.3.2. Boundary conditions

In the present study, the damper operation was modelled by prescribing a constant velocity at the moving boundary, representing the compression of the damper. The uniform inlet velocity value was defined to have uniform $\tilde{Q}$ relative volume flow rate distribution. Since the working fluid was considered incompressible, the pressure drop remained independent of the absolute pressure level. Therefore, a relative pressure of 0 Pa was imposed at the outlet. No-slip boundary conditions were applied to all solid walls to accurately capture the shear effects within the damping channel.

2.3.3. Numerical options, turbulence model

Turbulence modelling for non-Newtonian fluids presents a significant challenge, as conventional models such as *k-ϵ*, *k-ω*, and *SST* are primarily developed for Newtonian flows. Proper parameter tuning or the development of tailored turbulence models for non-Newtonian behaviour remains an active area of research. However, considering that the analytical approach assumes laminar flow and turbulence is not expected within the studied channel configurations, no additional turbulence model development was employed. Previous studies [18–20] have demonstrated that the SST k-ω model provides reasonable agreement with experimental data for pipe flows; therefore, this model was adopted with the recommended parameter settings. To accurately account for the non-Newtonian viscosity variations, the *strainRateFunction* transport model was employed in the CFD simulations. This approach allowed the viscosity to be directly interpolated from the experimental measurement data rather than relying on an analytical rheological model fit. It is important to emphasize that both the analytical and CFD models utilized raw, pointwise $\tau(\dot{\gamma})$ data instead of assuming a predefined constitutive equation. Numerical discretization schemes were selected to ensure stability and accuracy: the gradient term was

approximated using a Gauss linear scheme, while limited bounded Gauss was used for divergence terms. The Laplacian term was discretized with a Gauss linear orthogonal scheme, and linear interpolation was applied throughout the computational domain.

3. RESULTS

3.1. Rheological results

The rheological behaviour of the prepared STF samples was characterized using an Anton Paar MCR 301 rotational rheometer with a cone-plate measuring system. The viscosity as a function of shear rate was recorded in the range of 0.1 to 10,000 s^{-1} at a constant temperature of 25°C to ensure measurement accuracy and reproducibility.

The results indicate that the STF samples exhibit shear thickening behaviour, see Fig. 2. The flow curve can be divided into three distinct regions: (Region 1) a shear thinning region at low shear rates, (Region 2) a shear thickening region, and (Region 3) a second shear thinning region at higher shear rates. The most relevant segment for this study is the shear thickening region, where two key rheological parameters were identified: the critical shear rate ($\dot{\gamma}_c$), at which shear thickening begins, and the maximum viscosity (η_{max}), marking the end of the thickening process. Additionally, the dilatant effect, defined as the ratio of maximum viscosity to the viscosity at the critical shear rate, was determined as a significant characteristic parameter [21].

These findings confirm the pronounced shear thickening behaviour of the STF samples and highlight the importance of critical shear rate and maximum viscosity in understanding their rheological response. To establish a reference, the dispersion medium without silica—exhibiting Newtonian behaviour—was also measured. As shown in Fig. 2, the viscosity curves of the STF samples (12% and 15% silica concentration) are compared to the Newtonian fluid, illustrating the progressive shear thickening effect with increasing silica content. The addition of silica led to an increase in maximum viscosity and a decrease in the critical shear rate, suggesting that higher silica content results in stronger particle interactions and earlier hydrocluster formation. This rheological response plays a critical role in determining the fluid's performance in damping applications.

Table 1. summarizes the key rheological parameters for each STF sample, including the critical shear rate, maximum viscosity, dilatant effect, and the slope of the viscosity curve in the shear thickening region. These findings emphasize the significant role of silica concentration in modulating the shear thickening behaviour and provide valuable data for further analysis and modelling of STF behaviour in damping systems.

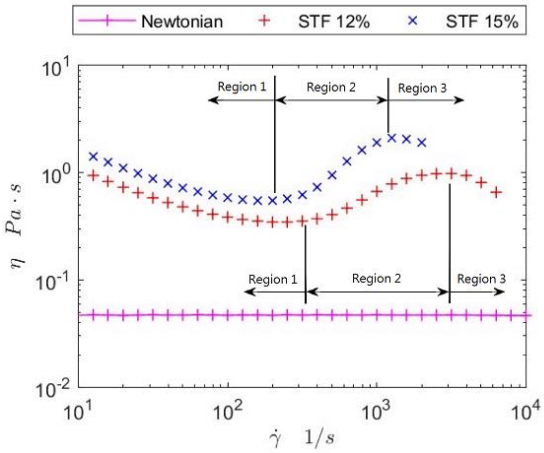

Figure 2. The rheological measurement data of the STF samples and the dispersion medium

Table 1. Critical and maximum rheological values of STF samples and the dispersion medium

	$\dot{\gamma}_c$ [1/s]	η_c [Pa·s]	$\dot{\gamma}_{max}$ [1/s]	η_{max} [Pa·s]	*dilatant effect*
PEG	-	0.46	-	0.46	-
STF12	251	0.35	3160	0.98	2.8
STF15	159	0.55	1260	2.1	3.8

3.2. CFD results

To evaluate the accuracy of the Hagen-Poiseuille equation in predicting the pressure drop across the pipe, CFD simulations were conducted for Newtonian and shear thickening fluids. The results were analysed for various pipe lengths and diameters, with a focus on the relative error

$$e = \left| \frac{\Delta p_{analytical} - \Delta p_{CFD}}{\Delta p_{CFD}} \right| \qquad (12)$$

between the analytical and numerical solutions. This relative error is plotted in the function of L/D relative length and $\tilde{Q} := \frac{Q}{2\pi R^3}$ relative volume flow rate.

3.2.1. Newtonian Fluid Case

Firstly, the flow of the pure PEG-200 liquid was investigated with the Newtonian viscosity of ($\eta = 0.46\ Pas$) In the first subplot of Fig. 3. we plotted the wall shear stress τ_w as a function of the relative flow rate Q̃. The analytical model gives a straight line according to the Eq. (10). The CFD results are marked with cross symbols, which exhibit the same linear relationship. For large L/D ratio the numerical values are aligning well with the analytical solution. However, the error increases as the L/D ratio decreases, indicating that shorter pipes introduce additional effects not accounted for by the Hagen-Poiseuille equation.

The second subplot in Fig. 3. shows the contour plot of the relative error e in the function of the relative volume flow rate and *L/D* ratio. The relative error primarily depends on the length-to-diameter

ratio (*L/D*) and the dependence on the volume flow rate is negligible.

Therefore, we also plotted the error for all of the simulation points in the function of the *L/D* in the third subplot. The points present a second order polynomial behaviour in the function of the *L/D* with R^2 = 0.95 determination coefficient.

As shown in Fig. 3., the error decreases with increasing *L/D*, indicating improved agreement between the analytical and CFD results for longer pipes. For *L/D* > 25, the relative error remains below 5%, suggesting that the Hagen-Poiseuille equation provides a reliable approximation in this range. However, for smaller *L/D* values, the influence of entrance and exit effects leads to higher discrepancies, emphasizing the need for alternative corrections in short pipe configurations.

3.2.2. Shear Thickening Fluid Case

For the shear thickening fluids with 12% (STF 12%) and 15% (STF 15%) concentration, we applied the same evaluation method as in the Newtonian case. Firstly, the flow curves were plotted in the first and second subplot of Figure 4. It is observable that the numerical values marked with cross demonstrate similar behaviour to the analytical curve.

However, the error of the analytical predictions shows a more complex behaviour due to the non-Newtonian viscosity variations. As depicted in the 3rd and 4th panels in Fig. 4, the relative error is strongly influenced by the relative flow rate $\tilde{Q}$ in addition to the *L/D* ratio. Three distinct regions were observed: In *Region 1* (low $\tilde{Q}$ before the thickening range) the error follows a trend similar to the Newtonian case, where longer pipes exhibit better agreement with analytical predictions while the volume flow rate has less significant effect. In *Region 2* (intermediate $\tilde{Q}$, in the thickening region) a sharp reduction in error is observed, likely due to the stabilizing effect of the shear thickening mechanism, which compensates for deviations from the Hagen-Poiseuille assumption. In *Region 3* (high $\tilde{Q}$): The error again follows the Newtonian trend, indicating that at sufficiently high flow rates, the deviations in viscosity do not significantly alter the pressure drop predictions.

A contour plot (Fig. 4) was generated to visualize the relative error as a function of *L/D* for relative volume flow rates corresponding to different regions. The results indicate that for shear thickening fluids, the Hagen-Poiseuille equation derived for the shear thickening fluid can be applied with reasonable accuracy for *L/D* > 50, provided that the flow rate remains outside the critical thickening.

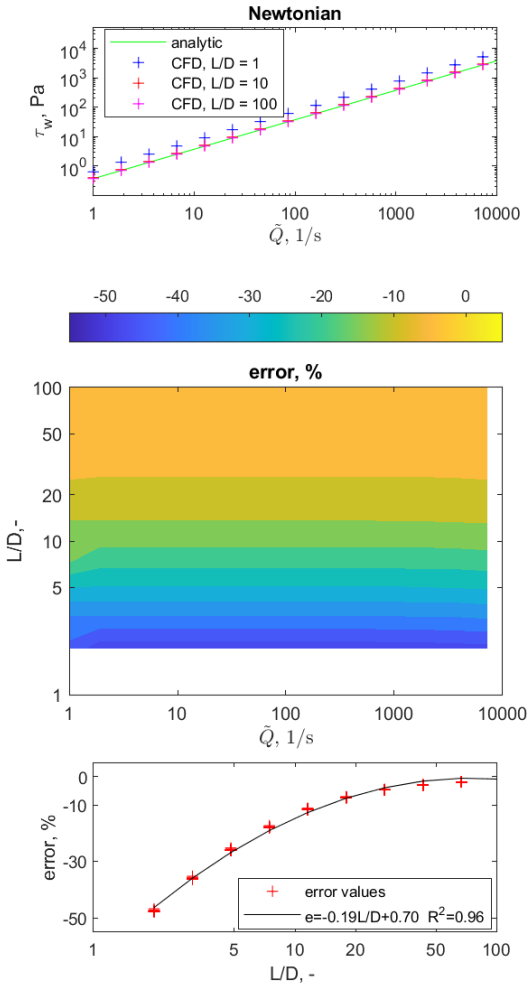

Figure 3. Relative error of the analytical model comparing to CFD results for Newtonian fluid

3.3. Application for Hydraulic Damper Design

The findings from this study provide critical insights into the applicability of the Hagen-Poiseuille law for damper design. For Newtonian fluids, analytical predictions are accurate for *L/D* > 25, while shorter pipes require correction factors to account for entrance and exit effects. For shear thickening fluids, the validity of the Hagen-Poiseuille equation depends not only on *L/D* but also on the flow regime. The equation holds for low and high flow rates but exhibits significant deviations in the thickening region. Industry designing hydraulic dampers with shear thickening fluids should ensure operation within the recommended *L/D* and relative volume flow rate ranges to maintain analytical accuracy.

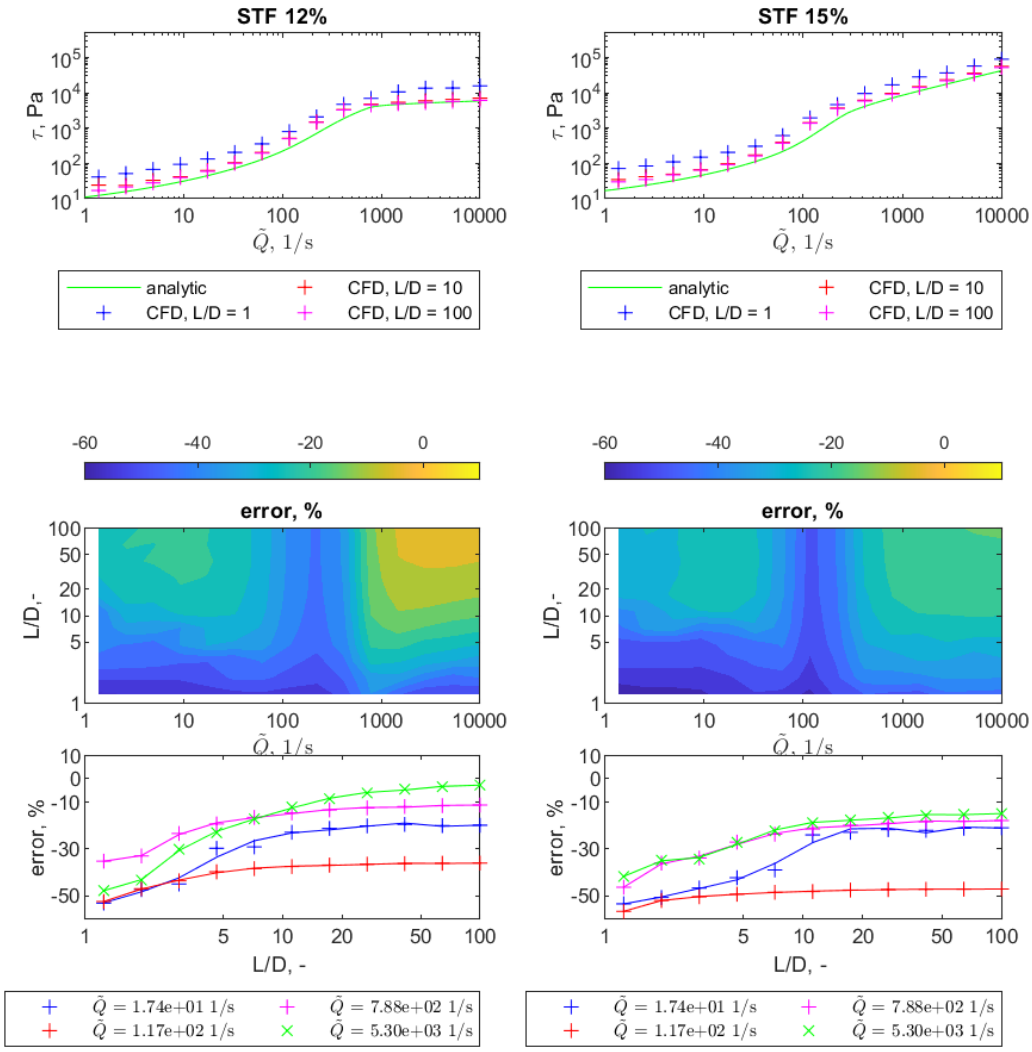

Figure 4. Relative error of analytical and CFD model results for STF12% and STF15%

4. CONCLUSIONS

This study systematically assessed the accuracy of the Hagen-Poiseuille equation in predicting the pressure drop for Newtonian and shear thickening fluids in a pipe flow representative of hydraulic dampers. To achieve this, we prepared shear thickening fluids and measured their rheological properties. We then conducted a series of CFD simulations to calculate the pressure drop for different volume flow rates and various pipe lengths. The error of the analytical approach was evaluated to identify the regions where the assumptions of the analytical derivation remain valid.

For Newtonian fluids, the accuracy of the Hagen-Poiseuille equation depends primarily on the length-to-diameter ratio, with $L/D > 50$ ensuring an error below 5%. For shear thickening fluids, the error is strongly dependent on the relative flow rate, with significant deviations occurring in the thickening region. The equation remains valid for $L/D > 50$ when and the wall shear stress is outside of the shear thickening region. The contour plot of relative error provides a practical guideline for determining the applicability of the analytical approach in damper design.

ACKNOWLEDGEMENTS

This work has been supported by the Hungarian National Research, Development and Innovation Centre under contract No. PD 146259.

REFERENCES

[1] Zhou, H.; Yan, L.; Jiang, W.; Xuan, S.; Gong, X.: Shear thickening fluid-based energy-free damper: Design and dynamic characteristics. Journal of Intelligent Material Systems and Structures, **27**, 208–220 (2016). http://doi:10.1177/1045389X14563869.

[2] Zhang, X. Z.; Li, W. H.; Gong, X. L.: The rheology of shear thickening fluid (STF) and the dynamic performance of anSTF-filled damper. Smart Materials and Structures, **17**

(2008). http://doi:10.1088/0964-1726/17/3/035027.

[3] Yang, J.; Sun, S.; Li, W.; Du, H.; Alici, G.; Nakano, M.: Development of a linear damper working with magnetorheological shear thickening fluids. http://dx.doi.org/10.1177/1045389X15577653, **26**, 1811–1817 (2015). http://doi:10.1177/1045389X15577653.

[4] Yeh, Y.; Chang, K.-C.; Chen, T.-W.: *Smart Viscous Dampers utilizing Shear Thickening Fluids with Silica Nanoparticles*;

[5] Wei, M.; Lin, K.; Guo, Q.; Sun, H.: Characterization and performance analysis of a shear thickening fluid damper. Measurement and Control (United Kingdom), **52**, 72–80 (2019). http://doi:10.1177/0020294018819543/ASSET/IMAGES/LARGE/10.1177_00202940188195 43-FIG8.JPEG.

[6] Wei, M.; Lin, K.; Liu, H.: Experimental investigation on hysteretic behavior of a shear thickening fluid damper. Structural Control and Health Monitoring, **26**, e2389 (2019). http://doi:10.1002/STC.2389.

[7] Gucuyener, I. H.; Gurcay, O. K.; Yanik, S.: A Comprehensive Evaluation of Rheological Models for Non-Aqueous Drilling Fluids. Proceedings of the International Conference on Offshore Mechanics and Arctic Engineering - OMAE, **10** (2022). http://doi:10.1115/OMAE2022-78546.

[8] Gómez, J. R.; Escandón, J. P.; Jimenez, E. M.; Torres, D. A.: Hydrodynamic Analysis of a Magnetorheological Squeeze Film Damper Using the Herschel-Bulkley Model and the Short Bearing Approximation. ASME International Mechanical Engineering Congress and Exposition, Proceedings (IMECE), **8** (2025). http://doi:10.1115/IMECE2024-144750.

[9] Hou, C.-Y.: Fluid Dynamics and Behavior of Nonlinear Viscous Fluid Dampers. http://doi:10.1061/ASCE0733-94452008134:156.

[10] Nagy-György, P.; Hős, C.: Predicting the damping characteristics of vibration dampers employing generalized shear thickening fluids. Journal of Sound and Vibration, **506**, 116116 (2021). http://doi:10.1016/J.JSV.2021.116116.

[11] Gao, H.; Chi, M.; Dai, L.; Yang, J.; Zhou, X.: Mathematical Modelling and Computational Simulation of the Hydraulic Damper during the Orifice-Working Stage for Railway Vehicles. Mathematical Problems in Engineering, **2020**, 1830150 (2020). http://doi:10.1155/2020/1830150.

[12] Zhao, Q.; He, Y.; Yao, H.; Wen, B.: Dynamic performance and mechanical model analysis of a shear thickening fluid damper. Smart Materials and Structures, **27** (2018). http://doi:10.1088/1361-665X/aac23f.

[13] Wei, M.; Lin, K.; Liu, H.: Experimental investigation on hysteretic behavior of a shear thickening fluid damper. Structural Control and Health Monitoring, **26** (2019). http://doi:10.1002/stc.2389.

[14] Galindo-Rosales, F. J.; Rubio-Hernández, F. J.; Velázquez-Navarro, J. F.: Shear-thickening behavior of Aerosil® R816 nanoparticles suspensions in polar organic liquids. Rheologica Acta, **48**, 699–708 (2009). http://doi:10.1007/s00397-009-0367-7.

[15] Fayed, H. E.; Sheikh, N. A.; Iliev, O.: On Laminar Flow of Non-Newtonian Fluids in Porous Media. Transport in Porous Media, **111**, 253–264 (2016). http://doi:10.1007/S11242-015-0592-8/FIGURES/7.

[16] Güzel, B.; Frigaard, I.; Martinez, D. M.: Predicting laminar–turbulent transition in Poiseuille pipe flow for non-Newtonian fluids. Chemical Engineering Science, **64**, 254–264 (2009). http://doi:10.1016/J.CES.2008.10.011.

[17] User Guide Available online: https://www.openfoam.com/documentation/user-guide (accessed on Feb 20, 2025).

[18] Csizmadia, P.; Hos, C.: CFD-based estimation and experiments on the loss coefficient for Bingham and power-law fluids through diffusers and elbows. Computers & Fluids, **99**, 116–123 (2014). http://doi:10.1016/J.COMPFLUID.2014.04.004.

[19] Csizmadia, P.; Till, S.; Paál, G.: CFD-based investigation on the flow of Bingham plastic fluids through 90 ∘ bends. Journal of the Brazilian Society of Mechanical Sciences and Engineering, **45**, 1–13 (2023). http://doi:10.1007/S40430-023-04121-0/FIGURES/10.

[20] Csizmadia, P.; Dombóvári, G.; Till, S.; Minkó, M.: CFD-based Estimation of Friction Factor in Rough Pipes with Herschel-Bulkley Fluids. Periodica Polytechnica Chemical Engineering, **67**, 74–82 (2023). http://doi:10.3311/PPCH.20857.

[21] David Moriana, A.: *Fabrication, characterisation and optimisation of shear thickening fluids*;